Coherent Multiple Imaging by means of Pupil Plane Filtering

Miklós Erdélyi, Armen Kroyan, Károly Osvay*, Zsolt Bor*, William L. Wilson,

Mike C. Smayling and Frank K. Tittel

Rice University, Electrical & Computer Engineering Department, MS 366 6100 Main, Houston, Texas

77005-1892

*Department of Optics and Quantum Electronics, JATE University H-6720 Szeged, Dóm tér 9, Hungary

ABSTRACT

A resolution enhancement technique suitable for Deep-UV microlithography based on coherent multiple imaging (CMI) will be described. We showed recently that a Fabry-Perot etalon inserted between the mask and the projection lens in an optical stepper is able to simultaneously enhance the resolution and depth of focus of an aerial image [1]. Since the multiple images of the mask pattern created by the etalon are added together coherently, the final image profile is very sensitive to the initial phase conditions. It is possible to simulate this coherent multiple imaging technique using a simulation model which either superimposes separate output electric fields or by applying an appropriate transmission-phase pupil plane filter in the simulator. The first approach, however, requires a modification of the simulation software which allows output of the electric field profile, while the second approach can be used with a conventional commercial lithography simulator.

In this paper computer simulations for isolated and extended contact hole arrays are used to demonstrate that the CMI method can enhance resolution by 18% while maintaining or even increasing the DOF of the aerial image. It is also shown that the high intensity side lobes generated by the filter can be eliminated by means of a phase shifting mask (π phase shift between the adjacent holes) or by reducing the spatial coherence of the illumination source. The optimum value of spatial coherence was found to be 0.28. In this case the side lobes disappear, and the intensity of the main peaks doubles. The impact of this technique on image intensity is also discussed.

1. INTRODUCTION

Coherent multiple imaging is a method for potentially enhancing both the depth of focus and resolution in optical microlithography. While a conventional projection process creates a single image of the photo mask, CMI produces several images shifted along the optical axis. A CMI technique that uses a Fabry-Perot etalon placed between the mask and the projection lens was demonstrated by the authors recently [1-3]. The resolution and depth of focus enhancement capabilities and the light loss of this method were evaluated theoretically and experimentally using simple mask patterns (on-axis contact hole, two contacts). However, the theoretical evaluation of extended, arbitrary mask patterns was not possible due to the limitations of the wave optics model which was used.

Part of the SPIE Conference on Optical Microlithography XII • Santa Clara, California • March 1999
SPIE Vol. 3679 • 0277-786X/99/$10.00

This paper reports on two approaches that can be used for evaluation of extended mask patterns by means of lithography simulation tools (Prolith/2, Solid-C). Attention will be focused on resolution and *DOF* enhancement, light loss and the problem of high intensity side lobes. Both isolated and extended periodical patterns will be discussed.

The first method is based on pupil-plane filtering that can be defined easily in most lithography tools. It was demonstrated that an appropriate phase-amplitude pupil-plane filter could substitute perfectly for a Fabry-Perot etalon placed between the mask and the lens. This paper will focus on the evaluation of two filters. A detailed analysis of these special pupil plane filters and their effect on the point spread function of the optical system can be found in Ref. 4.

The second method is based on superposition of the output electric fields produced by a Fabry-Perot etalon. Implementation of this method required a modification of the simulation software tools adding a capability of the electric field output. Using this new feature, we were able to develop a simulation model which is a direct simulation of the coherent multiple imaging technique.

2. IMPLEMENTATION OF A FABRY-PEROT ETALON BY MEANS OF A PUPIL PLANE FILTER

The theory of aerial image formation used by commercially available photolithographic tools is based on Fourier optics, and the electric field [E(x,y)] can be calculated by the following equation:

$$E(x,y) = \mathcal{F}^{-1} \cdot \{\mathcal{F}\{m(x,y)\} \cdot P(f_x, f_y)\}, \tag{1}$$

where $m(x,y)$ is the electric field transmittance of the mask pattern, $P(f_x f_y)$ is the coherent transfer function of the optical configuration of the stepper, and $\mathcal{F}$, $\mathcal{F}^{-1}$ represent the Fourier and inverse-Fourier transforms, respectively.

A Fabry-Perot interferometer placed between the mask and the projection lens generates several images of the original mask pattern whose axial distance is $2d$ and intensity ratio is R^2, where d is the separation and R is the reflectance of the etalon mirrors. Introducing a focal shift Δz, and a phase shift $\Delta\varphi$, the complex electric field behind the projection lens can be expressed in the form given in Ref. 5.

$$E(x,z) = e^{i\frac{4\pi(z-\Delta z)}{NA^2}} \cdot \int \mathcal{F}\{m(x,y)\} \cdot circ\ (r) \cdot e^{i2\pi r^2(z-\Delta z)} \cdot e^{i2\pi fx} \cdot e^{-i\Delta\varphi}\, df \tag{2}$$

where NA is the numerical aperture of the projection system, and $circ(r)$ is the transmission distribution of the lens. The spatial frequency (f), the focus shift (Δz) and the radial coordinate (r) are normalized by NA/λ, $2\lambda/NA^2$ and the pupil radius, respectively.
In the Fabry-Perot approach, the images behind the projection lens are shifted by $2dM^2$, $4dM^2$, $6dM^2$..., while the phase is shifted by φ, 2φ, 3φ..., and the amplitude ratio between the adjacent images is R. The total electric field is the superposition of fields described by Eq. 2, substituting the appropriate values of focal shift, phase and amplitude. The difference between the new and the original transfer functions (ΔP) can be expressed as follows:

$$\Delta P(r) = -R \cdot e^{-i\Phi} \cdot \frac{1}{R \cdot e^{-i\Phi} - 1}, \quad \text{where} \quad \Phi = \varphi - 2\pi\left(\frac{2}{NA^2} + r^2\right) \cdot 2dM^2. \tag{3}$$

The pupil radius (r) is divided into 100 equal parts and the normalized filter function is calculated in every segment.

A pupil plane filter defined in this fashion is equivalent to a Fabry-Perot etalon placed between the mask and the projection lens. Such a complex amplitude and phase filter is very similar to the transmission function of the Fabry-Perot simulated by the filter. This is due to the fact that a Fabry-Perot etalon can be regarded as a spatial filter that transmits certain spatial Fourier components (with appropriate phase shift) while blocking others. This similarity can make the filter optimization faster, since the optimum case (when the transmission amplitude maximum is close to the edge of the aperture) can be readily found.

Since the image separation ($2dM^2$) is insensitive to the phase, the relative image density (defined by the number of images in one DOF range: $N=DOF/2dM^2$) and the phase can be regarded as independent parameters of the system. While a 2π phase shift (equal to a 0.124 nm mirror shift) represents an entire period in phase, it has little effect on the image density. A detailed analysis of such a special pupil plane filter and its effect on the point spread function of the optical system can be found in Ref 5.

The input parameters used to run Prolith based simulations are the following:

Image Calculation mode: Full Scalar
Numerical Aperture (NA): 0.25
Reduction (1/M):10
Wavelength (λ): 248 nm (KrF excimer laser illumination)

In this paper two filters with relative image density of 5.3 and 10 (see Figure 1) are studied. The reflectance index (R) of the etalon mirrors simulated by the pupil plane filter is 0.95. Both filters are optimized so that the amplitude maximum is close to the edge of the aperture, so that the whole numerical aperture of the projection system is used.

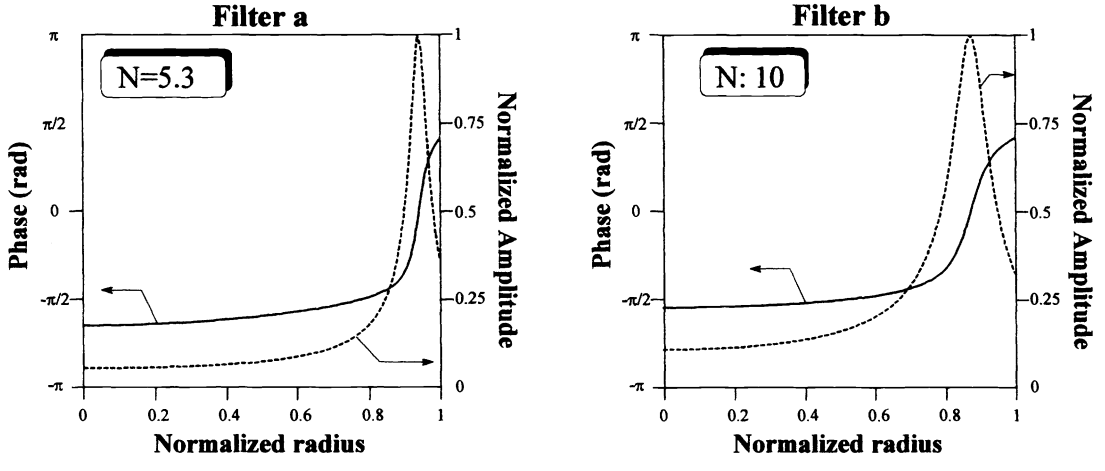

Figure 1. Normalized amplitude and phase distribution of the pupil-plane filters.

Although the characteristics of these filters are very similar, their effect on the final aerial image is very different. The amplitude ring of filter *a* is significantly narrower, and therefore it can be closer to the aperture (without serious cut-off) than in case of filter *b,* when the relative image density is 10. The closer

the ring is to the edge of the aperture, the larger the effective numerical aperture of the objective, and hence the resolution of the optical stepper is higher. On the other hand, the broader the width of the ring, the more light there is that can pass through the aperture resulting in a brighter image.

3. ISOLATED HOLE

The Rayleigh resolution limit ($W=0.61\lambda/NA$) using a projection lens with the input parameters defined above is 0.6 micron.

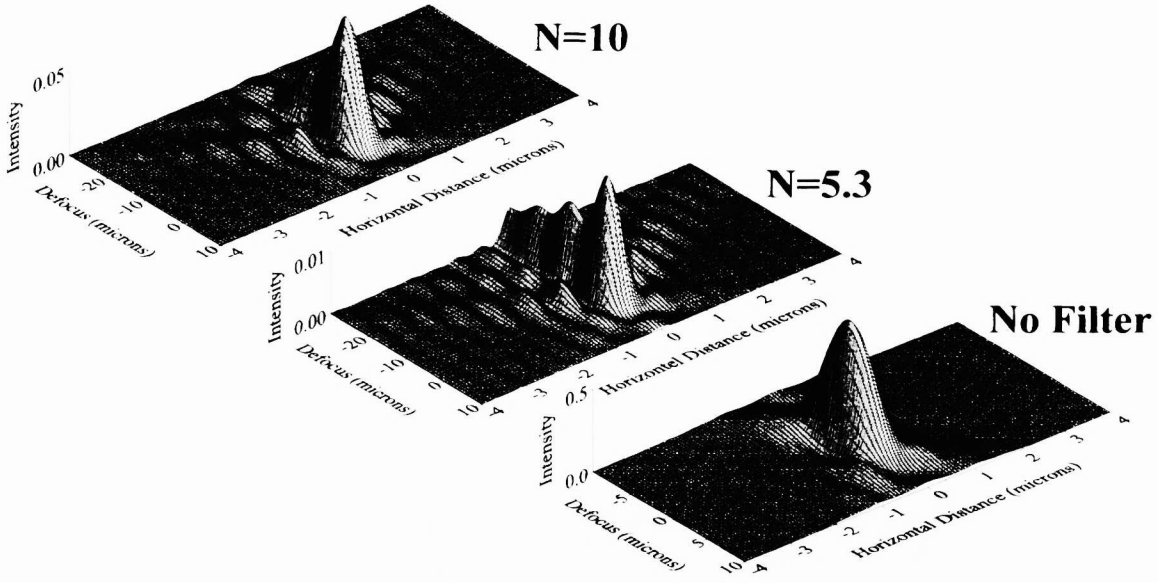

Figure 2. 3D aerial image of a 0.6 micron hole without filter and with filter *a* and *b*.

Figure 2 shows the 3D aerial images of a single 0.6 micron hole with and without filter. Without filter the aerial image is the well-known Airy pattern. The intensity distribution is symmetric and the main peak is located in the focal point. The intensity distribution changes drastically if a filter is used. Due to the constructive interference between the individual images, both the *DOF* and the resolution increase. However, the main peak is shifted toward the lens by about 5 microns; the intensity decreases; oscillations appear on the optical axis; and the side lobes increase. For the case of N=10, the image separation is almost half of that for the case of N=5.3. Therefore, the intensity decreases much faster on the optical axis. On the other hand, the intensity of the main peak is almost 5 times higher; about 10% of the original (Airy) intensity maximum. Figure 3 depicts the normalized cross sections of the intensity distributions (without filter defocus=0, with filter defocus=-5 microns). The FWHM of the main peak is 0.54 μm without the filter. Filters *a* and *b* introduce a resolution enhancement

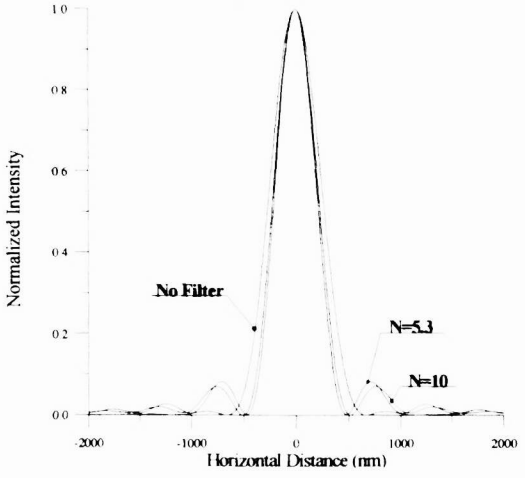

Figure 3. Normalized cross section with (def=-5 microns) and without filter (def=0)

of 20% and 15%, respectively. The resolution enhancement is larger when using filter *a* (N=5.3) since the amplitude maximum is closer to the edge of the aperture. On the other hand filters *a* and *b* impact the intensity distribution on the optical axis and the *DOF* (defined by the distance on the optical axis, where the intensity is larger than half of the main peak). The intensity distribution is not symmetrical with respect to the focal point, and the main peak is shifted by ~5 microns towards the lens. Without the filter, the *DOF* is ~7 microns (from -3.5 to 3.5 micron). While filter *b* does not change the original *DOF* value (from -1 to -8 micron), filter *a* increases the DOF to 16 microns (from -1 to -17 micron).

4. INTERACTION BETWEEN TWO CONTACT HOLES

Simultaneous imaging of contact holes is an issue due to side lobes which increase in intensity when using a Fabry-Perot filter. Figure 4 shows the 3D intensity distributions of two 0.6 micron contact holes separated by 0.6, 1, 1.4 and 2 microns, respectively. Without a filter, the intensity of the side lobes is very low (1.7% of the first one), and therefore their interference does not cause any serious problems. However, a filter can significantly change the aerial image. When the first and second side lobes overlap (space equals to 1 and 2 microns, respectively), high intensity peaks appear in the middle of the main peaks. The interference between the second and the first lobes does not cause high peaks, because there is a π phase difference between adjacent lobes. The last row in Figure 4 shows the case when a π phase shift was introduced between the two holes. In this case, the intensity is practically zero between the main peaks due to destructive interference.

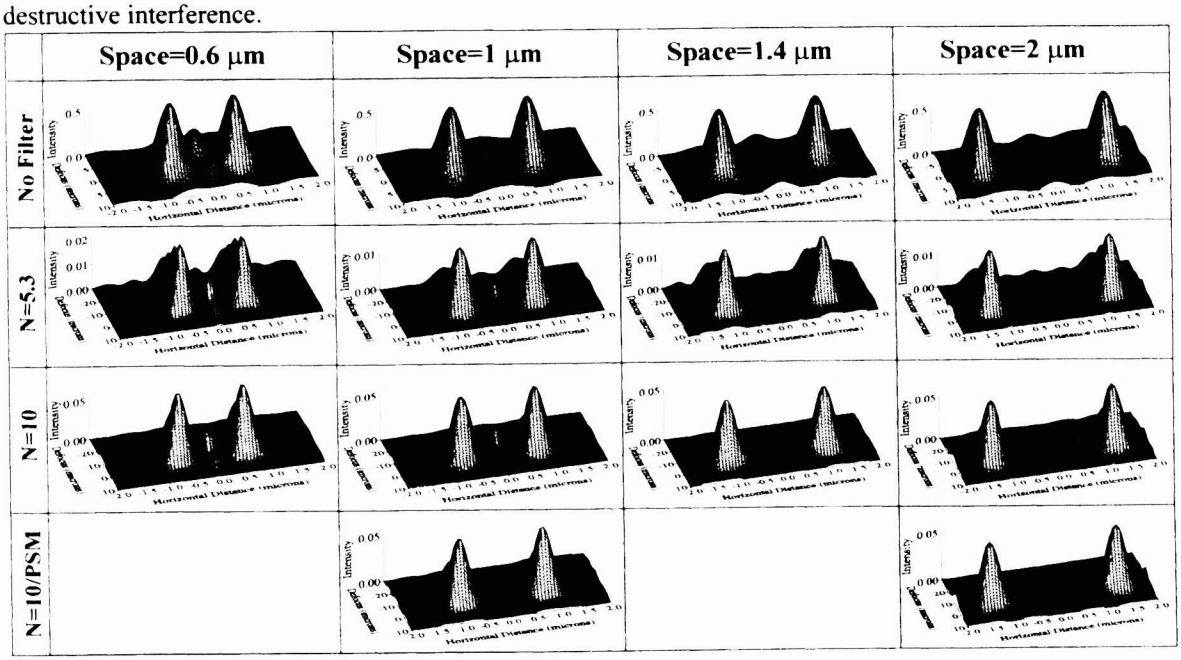

Figure 4. Interaction between two contact holes without (row 1) and with filters (row 2,3 and 4). The high intensity interference maxima between the main peaks (row 2 and 3) can be eliminated by means of a phase shifting mask.

A comparison of the intensity distribution of an isolated hole (Figure 2) and the hole pairs depicted in Figure 4 shows that the profile of the main peaks does not change. Therefore, every result for isolated holes is valid for the hole pairs. The filter enhances both the resolution and DOF simultaneously, and in conjunction with a phase shifting mask, undesirable high intensity interference maxima are eliminated.

5. IMAGING OF EXTENDED CONTACT HOLE ARRAYS

Since filter *a* introduces a significant loss of light (98%), only filter *b* was used to evaluate extended mask patterns. A 10x10 off-set contact hole array was defined with 0.5 micron holes. The x-y separation between the holes was 2.5 microns. The simulation results are depicted in Figure 5.

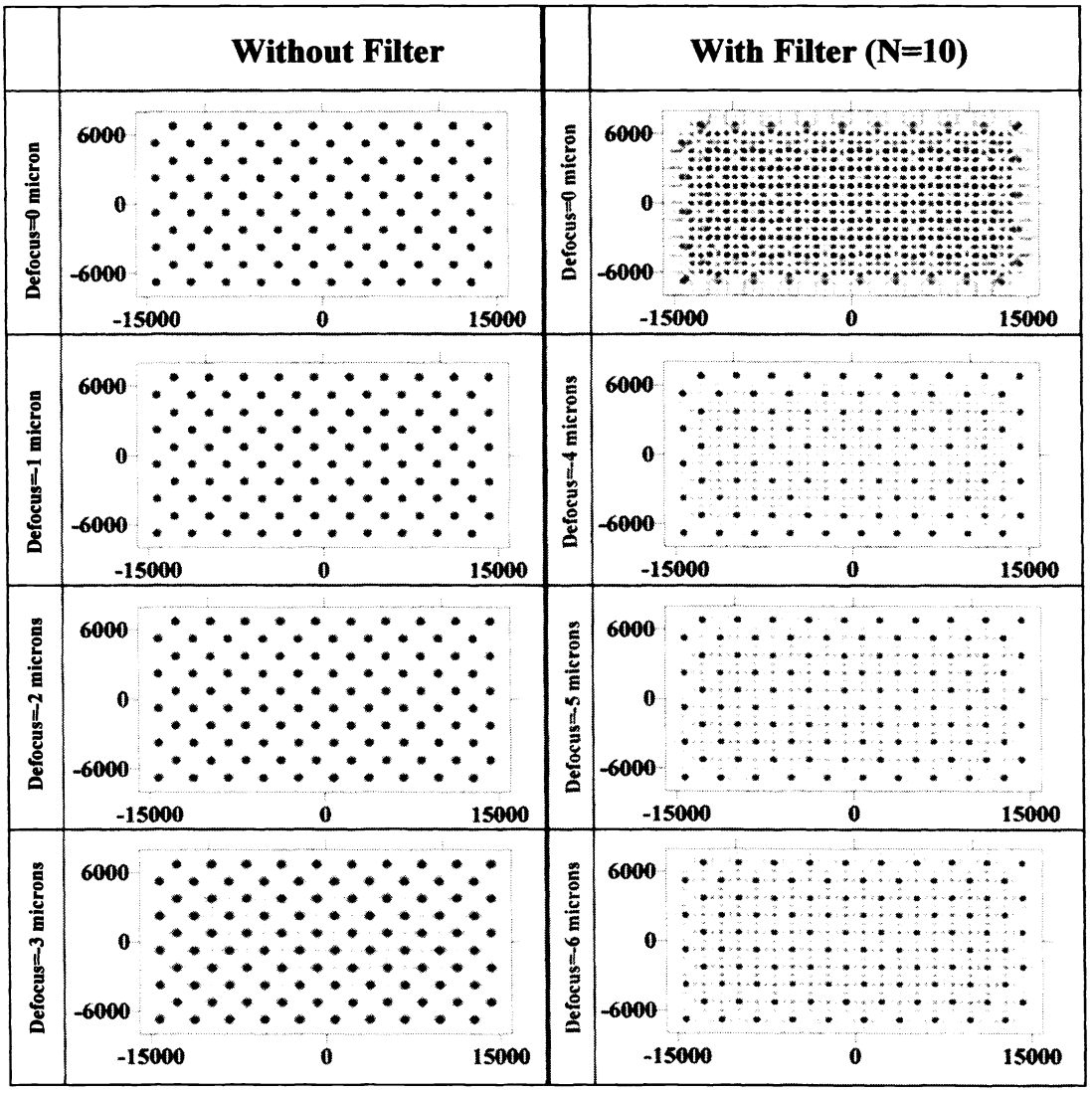

Figure 5. 2D simulation results of an extended off-set contact hole array with and without filter.

Without a filter, the intensity distribution is symmetrical to the focal point, since the optical system is free from optical aberrations. The FWHM of the holes is 0.56 μm and the *DOF* is 6 microns. Filter *b* shifts the intensity maximum by 5 microns towards the lens. The loss of light is almost the same as it was in the case of isolated contact holes. In the best focal plane (def=-5μm) the resolution enhancement is almost 18% (FWHM=0.46 μm) and the *DOF* is about 4 microns (from -3 to -7 micron). The *DOF* is limited by the increased secondary peaks placed between the main peaks, and not by their increased *CD*. These high intensity peaks are generated by the constructive interference between four second side lobes. Their

intensity is higher in the middle of the pattern than at the edge, where the diffraction ring systems can be observed clearly. (The rings are not perfect rings, since the holes have a square shape.)

Two different methods were proposed to decrease the intensity of the secondary peaks. Both methods use the fact that the high intensity interference peaks are the result of constructive interference. The first method decreases the spatial coherence of the illumination light so that the side lobes are not fully coherent. The interference peaks generated by partially coherent light have lower intensity. The second method does not change the spatial coherence (σ=0), but introduces a π phase shift between the adjacent holes (see previous section). Due to the destructive interference between opposite fields, the undesirable secondary peaks between the main maxima disappear. Figure 6 depicts how the intensity distribution depends on the spatial coherence of the illumination. The defocus was –5 microns. Using a totally coherent light source (σ=0), the side lobes are high. Decreasing the coherence of the light the intensity of the main peaks increases, and the side lobes practically disappear. The main peaks have maxima when the spatial coherence is 0.28. In the optimum case the peak intensity is almost doubled and reaches 13% of the original Airy maximum. The WFHM of the peaks does not change, but is essentially independent of spatial coherence. Figure 7 shows the normalized aerial image of an entire period of the mask for four different cases. Without (Airy pattern) and with filter *b* the defocus was 0 and –5 microns, respectively. The dotted curve shows the intensity distribution in the absence of a filter. The interference peaks generated by the second side lobes have relatively low intensity (12%), and cause no serious problems. However, using filter *b* in combination with coherent illumination (σ=0), the secondary peaks become almost 43% of the main peak (see dashed line). The combination of a filter and an appropriate spatial coherence can decrease the side lobes. The solid line shows the intensity distribution when the spatial coherence was 0.28. Similar results are obtained when the secondary peaks are eliminated by the introduction of a π phase shift between adjacent holes. In this case (see dash-dot line) the intensity is zero right in the middle of the main peaks. It is interesting that the FWHM of the main

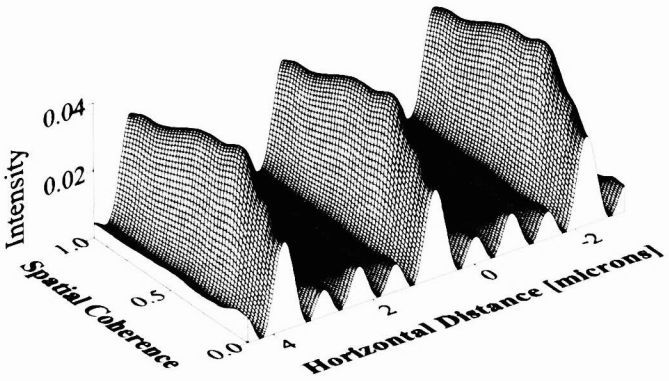

Figure 6. Aerial image versus spatial coherence.

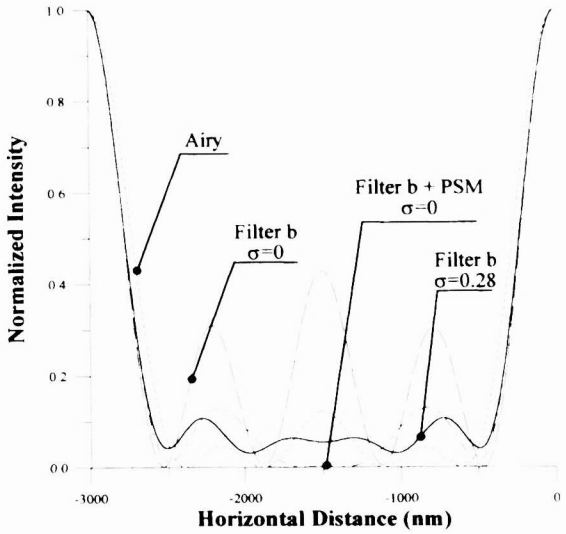

Figure 7. Aerial image without filter (dotted line); with filter using coherent light source (dashed line); with filter using partially coherent light source (solid line); and with filter using coherent light source and a phase shifting mask (dashed-dotted line).

peak does not change when either the spatial coherence or the phase between the holes varies. The resolution enhancement is introduced by the filter. The phase mask without filter does not change the resolution.

6. SECOND SIMULATION METHOD OF THE COHERENT MULTIPLE IMAGING TECHNIQUE

We have developed another method which simulates the impact of a Fabry-Perot etalon on lithographic optical imaging. In order to directly simulate the CMI technique, one must add the electric field profiles from several images, preserving both intensity and phase. Normally this is not possible, as most commercial lithography simulators only provide the final aerial intensity as an output. Specifically for this study however, FINLE Technologies and Sigma-C, provided modified software packages which enabled us to access the electric field profiles directly, and hence directly simulate the CMI technique.

As discussed in section 2, a Fabry-Perot etalon generates several images of the original mask pattern which are appropriately related to each other in terms of their phase, intensity, and separation distance. Based on these relationships, we have developed a program which calculates the input parameters and generates appropriate electric field profiles for each image at a specified focal plane. This program then superimposes the various profiles, resulting in a final image at a given focal plane. It is necessary to superimpose at least 40 electric field distributions in order to obtain the enhanced aerial image in one focal plane with a high level of precision.

The results obtained using this simulation method are in agreement with the theoretically predicted profiles and as well as simulations based upon pupil plane filtering. Using the same input parameters in Prolith/2 as in the previously discussed simulation approach (section 2), the FWHM of an isolated 0.6 μm contact hole measures 0.54 μm without the Fabry-Perot etalon. Simulation results with the etalon showed that when optimal $\Delta\varphi$ phase shift values are used, the FWHM can be enhanced to 0.44 μm and 0.45 μm for $\Delta\varphi = 30^0$ and $\Delta\varphi = 25^0$ respectively (Figure 8). Resolution enhancements in these cases are 16.7 % and 18.6 % respectively. It was observed that the optimal focal plane shifts from defocus = 0 to defocus = -4 microns plane. In this plane the intensity loss due to the etalon is measuring 89 % and 86.6 % for $\Delta\varphi = 30^0$ and $\Delta\varphi = 25^0$ respectively. Also the FWHM resolution enhancement is further improved to 0.385 μm (28.7 %) and 0.425 μm (21.3 %). The relative image density in both

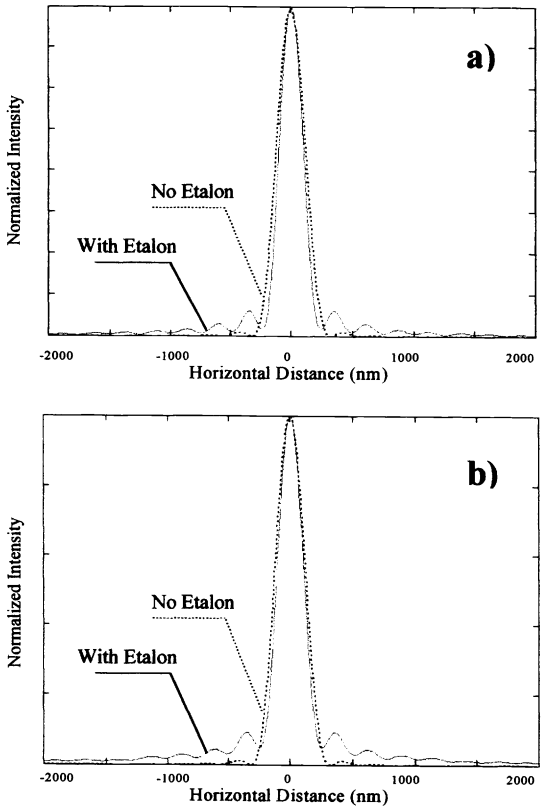

Figure 8. Aerial images of a 0.6 μm isolated contact hole without etalon (dotted line) and with etalon (solid line): **a)** $\Delta\varphi = 30^0$ and **b)** $\Delta\varphi = 25^0$.

cases is about 8. The depth of focus enhancement in both cases is about 200%.

The coherent multiple imaging method represents another proof of the results obtained theoretically or through simulations based on pupil plane filtering. Figure 9 shows a comparison of results obtained using both simulation approaches. However, the electric field superposition method has some disadvantages compared to the pupil plane filter approach. Both Prolith and Solid-C can only output an electric field profile when the illumination source is perfectly coherent. Another disadvantage is the overall calculation speed. Instead of a single run as in the case with the pupil plane filtering approach, the electric field superposition method requires multiple separate electric fields to be generated and then superimposed in order to obtain the final image.

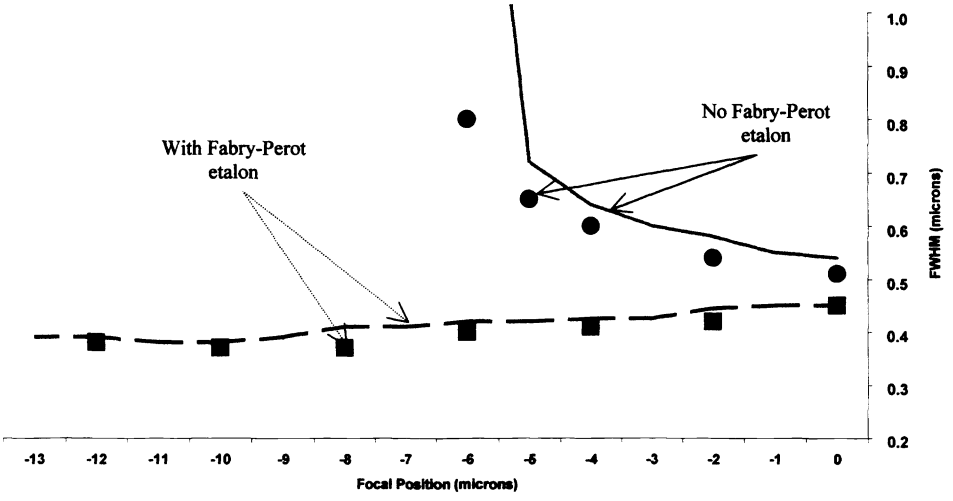

Figure 9. A comparison of FWHM through focus using pupil plane filtering (markers) and coherent image superposition (lines) simulation approaches.

7. CONCLUSION

A resolution enhancement technique suitable for Deep-UV microlithography based on coherent multiple imaging was evaluated using Prolith/2. A Fabry-Perot etalon that generates multiple images was simulated by an appropriate phase-amplitude pupil plane filter. Simulations for isolated and extended contact hole arrays demonstrated that this method can enhance resolution by 18% while maintain or even increase the DOF of the aerial image. It was also shown that the high intensity side lobes generated by the filters can be eliminated by means of a phase shifting mask (π phase shift between the adjacent holes) or by reducing the spatial coherence of the illumination light. The optimum value of spatial coherence was found to be 0.28. In this case the side lobes disappear, and the intensity of the main peaks is doubled. However, even in this optimum case the peak intensity is only 13% of the original Airy peak. The main source of light loss is that the transmission ring generated by the high reflectivity mirrors (R=0.95) is very narrow. A filter with smaller light loss is likely to be generated by an optimization process that requires a reflectivity change of the Fabry-Perot mirrors.

Direct simulation method for the coherent multiple imaging technique was also developed. The results obtained using this method either with Prolith or Solid-C show a good agreement with the ones obtained theoretically or based on pupil plane filtering.

ACKNOWLEDGEMENT

This research was supported in part by the Texas Instruments Inc. University Research program and by the OTKA Foundation of the Hungarian Academy of Sciences (T020910). We would like to thank FINLE Technologies and Sigma-C for providing their support.

REFERENCES

1. M. Erdelyi, Z. L. Horvath, G. Szabo, Zs. Bor, F. K. Tittel, Joseph R. Cavallaro, Michael C. Smayling: Generation of Diffraction-Free Beams for Applications in Optical Microlithography, *J. Vac. Sci. Technol.* B 15(2) Mar/Apr 287-292 (1997).
2. Z. L. Horvath, M. Erdelyi, G. Szabo, Zs. Bor, F. K. Tittel and J. R. Cavallaro: Generation of nondiffracting Bessel Beams with Fabry-Perot interferometer, *J. Opt. Soc. Am.* A, 14(11), pp.: 3009-3013, (1997)
3. M. Erdelyi, Z. L. Horvath, Zs. Bor, G. Szabo, J. R. Cavallaro, Michael C. Smayling and F. K. Tittel: Optical microlithography with nearly nondiffracting beams, Optical Microlithography X, Santa Clara, CA (March 9-14, 1997); SPIE Proc. 3051, 959-966, (1997)
4. M. Erdelyi, Zs. Bor, William L. Wilson, Michael C. Smayling and Frank K. Tittel: Simulation of Coherent Multiple Imaging by means of Pupil Plane Filtering in Optical Microlithography, (submitted to JOSA A, 1999)
5. H. Fukuda, T. Terasawa and S.Okazaki, "Spatial filtering for depth of focus and resolution enhancement in optical lithography", *J. Vac. Sci. Technol. B*, **9(6),** pp. 3113-3116, 1991.